JOURNAL OF COMPUTATIONAL PHYSICS 103, 450–464 (1992)

A New Lagrangian Method for Steady Supersonic Flow Computation Part II. Slip-line Resolution

W. H. HUI AND C. Y. LOH

Department of Applied Mathematics, University of Waterloo, Waterloo, Ontario, Canada N2L 3G1

Received April 26, 1990; revised December 4, 1990

It is well known that high-order accurate shock-capturing schemes, e.g., second-order TVD and ENO schemes, based on Eulerian formulation are capable of resolving a shock discontinuity in two grid points, but they smear a slip-line (contact-line) discontinuity over several grid points. In this paper we show theoretically and numerically that the first-order Godunov scheme based on the new Lagrangian formulation of Hui and Van Roessel for steady supersonic flow always resolves an isolated slip-line discontinuity crisply, provided it is initially aligned with a grid line. Moreover, a simple extension of the second-order scalar TVD scheme of Sweby to the system of Euler equations based on the new Lagrangian formulation, with no special procedure for slip-line detection, resolves slip-line discontinuities in at most two grid points. Many examples are given, showing excellent agreement with known exact solutions.

1. INTRODUCTION

Important advances have been made on the numerical simulations, using a shock-capturing methodology, of inviscid gas flow as governed by the Euler equations of motion. This is most evident in the recent comprehensive survey article by Yee [1].

It appears that most existing work is based on Eulerian formulation of fluid motion. It has also become traditional to treat steady flow as an asymptotic state of an unsteady flow after marching a large number of time steps, although Roe [2] has recently suggested that the time has come to reappraise this traditional approach.

In the special case where the flow is everywhere supersonic, steady flow can be easily computed as steady flow proper without artificially introducing the time variable. This is possible because the governing Euler equations for steady supersonic flow are of hyperbolic type, and thus one of the spatial variables can be used as a time-like variable. In this way, computer storage and time can be greatly reduced and accuracy increased. Glaz and Wardlaw [3] and Pandolfi [4] have taken this approach with success.

Supersonic flows are usually dominated by shock and slip-line (contact line) discontinuities. Woodward and Colella [5] observed, after reviewing three decades of research efforts in simulating such flows, that the overall accuracy of such (numerical) simulations is very closely related to the accuracy with which flow discontinuities are represented.

It has now been well established (see Harten [6] for ideal gas flow and Liou *et al.* [7] for real gas flow) that with a second-order total variation diminishing (TVD) scheme or, better still, with a higher order essentially non-oscillatory (ENO) scheme, Eulerian formulation is capable of resolving a shock discontinuity in 1D unsteady flow in about two computation cells (two grid points). However, resolution of slip-line (contact-line) discontinuities in the Eulerian formulation is rather poor; it typically takes six or more cells to resolve it [6, 7].

Based on the new Lagrangian formulation developed by Hui and Van Roessel [8, 9], the present authors [10, referred to as Part I hereafter] have applied the first-order Godunov scheme to compute two-dimensional steady supersonic flow. In this formulation the two independent variables are a stream function ξ and the Lagrangian time τ, the latter playing a dual role as the Lagrangian label of a fluid particle while being the time of motion. Consequently a steady flow is computed, by marching in τ in a way similar to 1D unsteady flow, as a steady flow proper and not as the asymptotic state of an unsteady flow. It has been shown in Part I that the new Lagrangian method provides an alternative, and is potentially advantageous, to the Eulerian method, especially in resolving slip-line discontinuities.

In this paper we first show theoretically and confirm numerically that the first-order Godunov scheme based on the new Lagrangian formulation for steady supersonic flow always resolves an isolated slip-line discontinuity crisply, provided it is initially aligned with a grid line. Furthermore, we demonstrated that a straightforward extension of Sweby's [11] second-order scalar TVD scheme to the system of Euler equations in the new Lagrangian formulation, with no special procedure for slip-line detection, always resolves a slip-line in at most two points. Many examples are given.

0021-9991/92 $5.00

2. ON THE NUMERICAL RESOLUTION OF A SLIP-LINE (CONTACT-LINE) DISCONTINUITY

As mentioned earlier, in any shock-capturing computation based on the Eulerian formulation a slip-line discontinuity is typically smeared over six or more grid points [6, 7]. This in fact grows worse with increasing time τ like $O(\tau^{1/(r+1)})$, where r is the formal order of accuracy of the numerical scheme used. To remedy this, Harten [12] suggested using artificial compression, which has been followed by Shu and Osher [13]. Harten [14] recently further developed a technique of sub-cell resolution. These techniques, when applied to high order ENO schemes, have greatly improved the resolution of slip-line discontinuities. However, they require detection of the slip-line location which tends to complicate the logic in the computer code and is not always reliable in a complex flow field. Moreover, any artificial compression technique contains some free parameter, representing the degree of compression, whose value has to be determined case-by-case. Thus, in cases where an exact solution is not available for such "tuning," there is a danger of over-compression in parts of the flow field.

In this section we shall first review the properties of a slip-line in steady flow, by contrasting them with those of a shock, and then show that isolated slip-line discontinuities can be resolved crisply using the Godunov scheme based on the new Lagrangian formulation, provided the slip-line initially coincides with a computational cell boundary.

Flow discontinuities are classified as shock and slip-line (including the special case of contact-line) discontinuity. Across a shock the tangential component of flow velocity is continuous while all other flow variables experience a jump. In contrast, across a slip-line the pressure p and the flow inclination $\theta = \tan^{-1}(v/u)$ are continuous (u and v denote the x- and y-components of flow velocity, respectively), while all other variables, e.g., density ρ, flow speed $q = \sqrt{u^2+v^2}$, Mach number M, and specific entropy S (defined as p/ρ^γ) experience a jump. A slip-line is also a streamline, whereas a shock line cannot be a streamline. Consequently, two shocks mah intersect, but two slip-lines never intersect, and slip-lines are thus necessarily isolated. A shock can be generated either suddenly or gradually (through convergence of Mach lines) but a slip-line can be generated only suddenly as a result of the interaction of two different flows, or the intersection of two shocks, or the sudden birth of a shock of finite strength in the interior of the flow field (an example of which is given in Appendix A). The strength of a shock can vary along the shock line; in particular, it may diminish to a Mach line. In contrast, the strength of a slip-line, as measured by the entropy jump across it, remains constant in between two shocks. This is a consequence of the constancy of entropy along a streamline in steady flow.

In short, a slip-line is generated suddenly and, once generated, its strength remains unchanged until it meets a shock. Consider now two different uniform flows separated by a slip-line. They must have the same pressure and the same flow direction. Therefore, they do not affect each other in any way while moving alongside each other until the slip-line intersects a shock or other waves. This is just a direct mathematical result of the Euler equations of motion of an invisced fluid (but is not true of the Navier–Stokes equations for a viscous fluid).

This physical property of the flow in the neighborhood of an isolated slip-line is modeled *exactly* by the Godunov scheme based on the new Lagrangian formulation. In this formulation the Euler equations of motion of a perfect gas obeying a γ-law in conservation form are (Part I, Eqs. (21))

$$\frac{\partial \mathbf{E}}{\partial \tau} + \frac{\partial \mathbf{F}}{\partial \xi} = 0, \tag{1}$$

where

$$\mathbf{E} = \begin{pmatrix} K \\ H \\ Ku + pV \\ Kv - pU \\ U \\ V \end{pmatrix} \equiv \begin{pmatrix} e_1 \\ e_2 \\ e_3 \\ e_4 \\ e_5 \\ e_6 \end{pmatrix}, \quad \mathbf{F} = \begin{pmatrix} 0 \\ 0 \\ -pv \\ pu \\ -u \\ -v \end{pmatrix} \equiv \begin{pmatrix} f_1 \\ f_2 \\ f_3 \\ f_4 \\ f_5 \\ f_6 \end{pmatrix} \tag{2}$$

$$K = \rho(uV - vU) \tag{3}$$

$$H = \frac{1}{2}(u^2+v^2) + \frac{\gamma}{\gamma-1}\frac{p}{\rho} \tag{4}$$

$$u = \frac{\partial x}{\partial \tau}, \qquad v = \frac{\partial y}{\partial \tau} \tag{5}$$

$$U = \frac{\partial x}{\partial \xi}, \qquad V = \frac{\partial y}{\partial \xi} \tag{6}$$

and x and y are the cartesian coordinates of a fluid particle. According to the Godunov scheme (Part I) the outcome of the interaction of two different uniform flows $\mathbf{Q}_A$ and $\mathbf{Q}_B$ separated by a slip-line at time τ is the solution to the Riemann problem with $\mathbf{Q}_A$ and $\mathbf{Q}_B$ as initial data. Here $\mathbf{Q} = (u, v, p, \rho)^T$. This solution is exact and yields the same $\mathbf{Q}_A$ and $\mathbf{Q}_B$ as the new uniform flows at time $\tau + \Delta\tau$, $\Delta\tau$ being subject to the usual CFL stability condition. (The only possible error in computing flow states at $\tau + \Delta\tau$ from those at τ is due to computer round-off, which we shall neglect). Now, since in the new Lagrangian cell advances in time τ along a streamline with flow velocity (Eqs. (5)), it thus behaves literally as a fluid particle and the same cell can be identified with one and the same particle for all time. The cells adjacent to a slip-line—a streamline—never cross it but remain adjacent to it. The above procedure can therefore be

repeated until the slip-line meets a shock or other waves, showing that an isolated slip-line discontinuity is resolved crisply, provided it is initially taken as a cell boundary.

By contrast, the computational cell in the Eulerian method (see [3, 4]) advances in a fixed direction in space, the x-direction say, which in general does not agree with the flow direction. Consequently, cells near a slip-line will cross it, and hence the Godunov cell-averaging scheme will smear the slip-line, rendering its resolution rather poor.

The above discussions show clearly why the new Lagrangian method with Godunov scheme models the flow adjacent to a slip-line most honestly and, hence, why it is superior to the Eulerian method. This method of using streamlines as coordinate lines does, however, have a problem of its own; namely, cells on the opposite sides of a slip-line advance at different flow speeds and hence tend to lose contact with each other physically. But this is easily remedied by choosing different time steps $(\Delta\tau)_+$ and $(\Delta\rho)_-$ for the two sides (denoted as "+" side and "−" side) such that

$$q_+(\Delta\tau)_+ = q_-(\Delta\tau)_-. \tag{7}$$

In this way, cells on directly opposite sides of a slip-line will remain so for all time and the physics of the flow is correctly modeled by the numerical scheme.

In Fig. 1 the evolution of a slip-line in an otherwise continuous flow is illustrated. $\gamma = 1.4$ is used in all computations

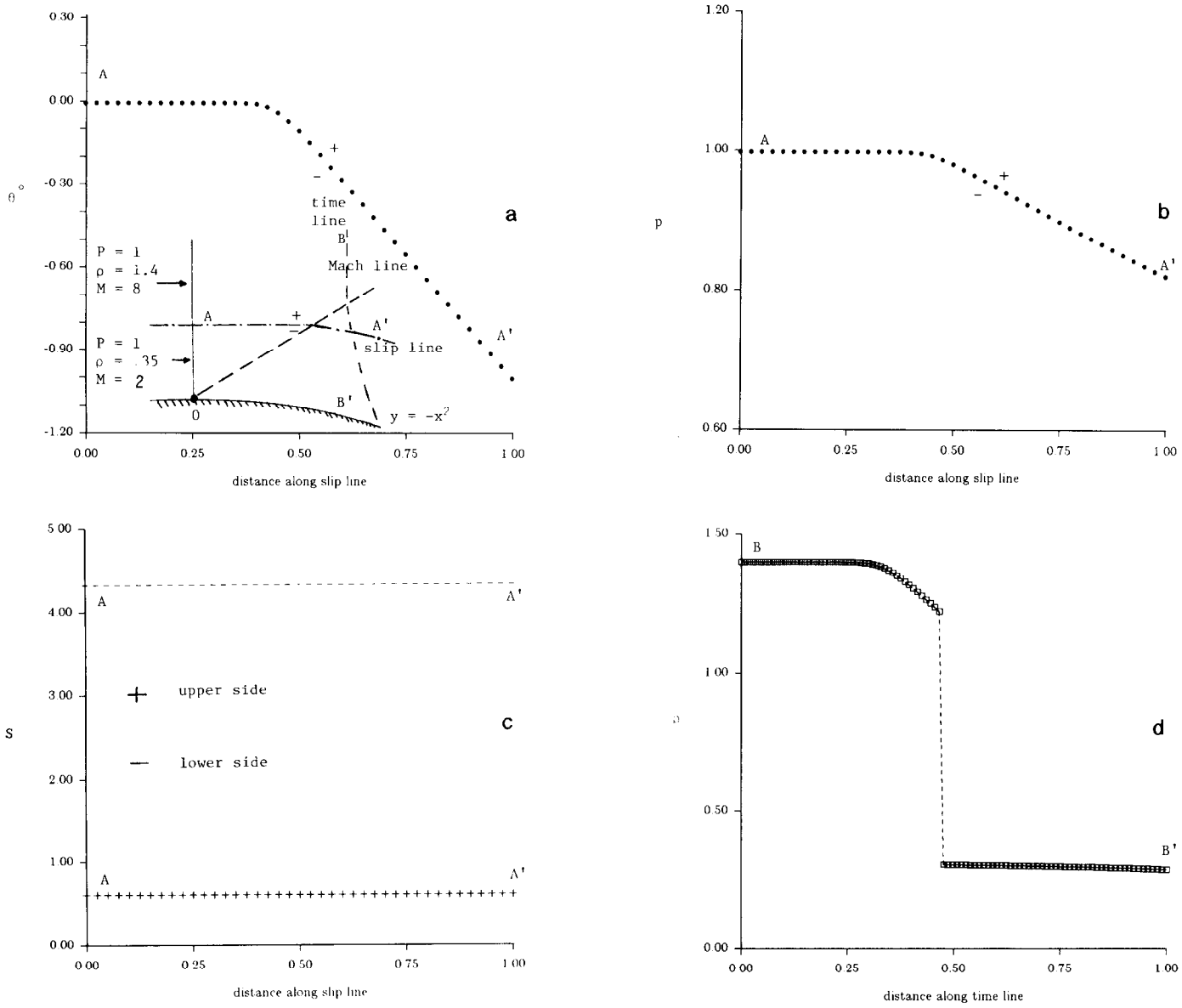

FIG. 1. Slip-line Evolution, first order Godunov scheme. (a)–(c) computed flow variables along the slip-line AA'; (a) flow inclination; (b) pressure; (c) entropies; (d) computed density along a typical time line BB'.

of this paper. The flow variables on one side of the slip-line are $p=1$, $\rho=1.4$, $u=8$, $v=0$ (hence, $M=8$, $S=0.6243$), whereas on the other side they are $p=1$, $\rho=0.35$, $u=4$, $v=0$ (hence $M=2$, $S=4.3482$). The shape of the solid wall is given by $y=-x^2$. A grid of 100 uniform cells of width $h=0.0002$ is used in the computation using the first-order Godunov scheme based on the new Lagrangian formulation (Part I). Fifty cells are placed above the slip-line and the other 50 cells are below it, and the slip-line is taken to coincide with the interface boundary between two cells. The computed evolution along the slip-line of the flow inclination θ, pressure p, density ρ, and entropy S are shown in Figs. 1a–c, whereas the density distribution along a typical time line are shown in Fig. 1d. It is clear from these figures that the slip-line remains invariant until the first Mach line from the point 0 begins to affect it and that the slip-line is resolved crisply.

The evolution of the same initial slip-line is next studied using 100 uniform cells with the same width h, but the slip-line is now taken not to coincide with a cell boundary. Instead, it initially lies inside the 51st cell at 0.65 h above the cell's lower boundary and 0.35 h below its upper boundary. (A new cell of width 0.65 h is inserted adjacent to the solid wall.) This situation arises more naturally in numerical computations of complex flow fields that do not employ special procedure for slip-line detection. Our computations

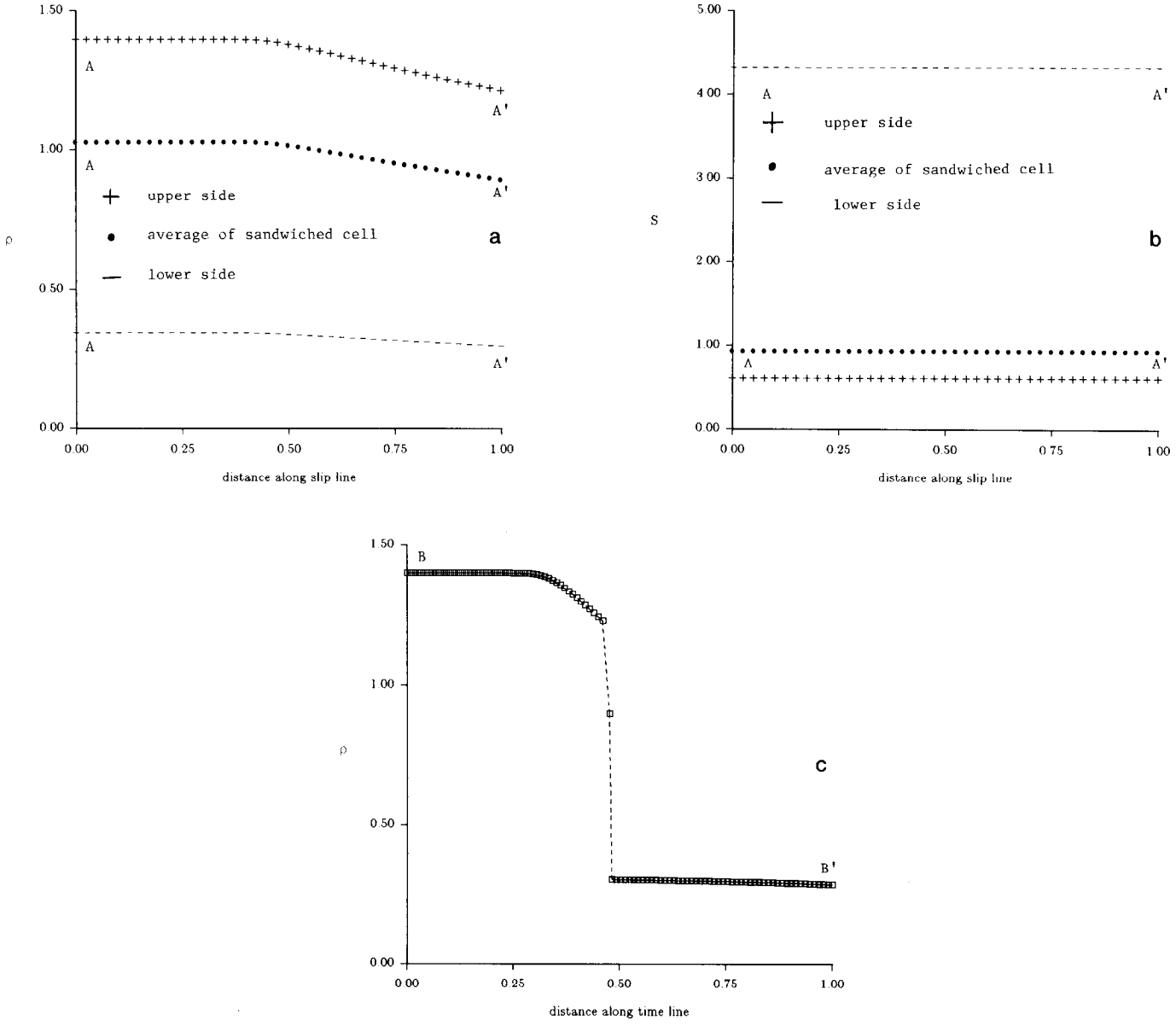

FIG. 2. Evolution of a slip-line, whose initial position does not coincide with a cell boundary. (a)–(b) computed flow variables along the slip-line; (a) densities; (b) entropies; (c) computed density along a typical time-line BB' (see Fig. 1a).

show that a slip-line whose initial position lies inside a computational cell immediately splits itself into two adjacent slip-lines aligned with the boundaries of the cell containing the original slip-line (Figs. 2a–b). The sum of the jumps of a flow variable across those two slip-lines is also found to be equal to the original jump. Figure 2c plots the distribution of density along a typical time line which clearly shows that the original slip-line, whose position is not taken to be a cell boundary, is smeared numerically over one grid point.

It is evident from the above theoretical discussions and numerical examples that Godunov scheme based on the new Lagrangian formulation resolves isolated slip-line discontinuities in the otherwise continuous flow crisply, provided the initial slip-line is taken to be a cell boundary. Smearing of a slip-line can, therefore, only come from the errors of the initial data or from its non-alignment with a cell boundary. Thus in the case of shock–shock interaction of Example 4 of Part I, the jump of a flow variable across neighboring cells near the interaction point is reduced (to the level of the difference of two shock jumps) at interaction and the first-order Godunov scheme smears the shock over only two grid points (Fig. 4a, Part I). The resulting slip-line is consequently also smeared over two grid points only (Figs. 4e–f, Part I). On the other hand, in the case of overtaking of shocks of Example 5 of Part I, the jump of a flow variable across neighboring cells near the interaction point is greatly increased (to the level of the sum of the strengths of the two shocks) at overtaking and the first-order Godunov scheme smears it to about eight points (Fig. 5a, Part I). As a consequence of this inaccuracy of the initial data, the slip-line generated due to shock–shock overtaking is also smeared over eight points, as is clearly shown in Fig. 5d of Part I.

Clearly, then, to better resolve slip-line discontinuities numerically it is desirable to align a slip-line at its birth with a cell boundary in the computation. However, this requires a special procedure for slip-line detection which not only would complicate programming logic but also could be unreliable in complex flow fields. On the other hand, we have found (Section 3), after computer experiments with large number of examples, that once the Godunov scheme is upgraded to a high resolution TVD scheme the shocks are always resolved by two grid points while the slip-lines are resolved even more accurately—in most cases by only one grid point— with no detection procedure. This is clearly demonstrated in Fig. 3 which shows the Mach number variation along a slip-line after the overtaking of shocks. This is the case in Fig. 5d of Part I recomputed using the high resolution TVD scheme (explained in Section 3). The shock and the slip-line are now both resolved by one grid point without employing any procedure for detecting them, in direct contrast to the eight-point resolution of the slip-line in Part I (Fig. 5d).

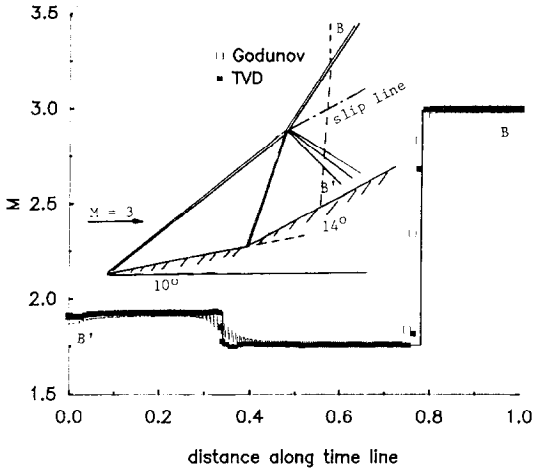

FIG. 3. Overtaking of shocks. Mach number distribution along a time line BB', showing the resolution of slip-line with a high resolution TVD scheme. The slip-line resolution is greatly improved over the first-order Godunov scheme of Part I, Fig. 5d.

3. APPLICATION OF HIGH RESOLUTION TVD SCHEME

3.1. *The Updating Formula*

The first-order Godunov scheme in practice is notedly inaccurate and needs to be upgraded to higher order accuracy. There now exist many such high resolution schemes. In this paper, we shall extend the second-order accurate scalar TVD scheme of Sweby [11] to the Euler equations in our new Lagrangian formulation.

Classical second-order schemes, e.g., the well-known Lax–Wendroff scheme, when applied to the Euler equations produce pre-discontinuity and post-discontinuity oscillations which are non-physical and can cause computations to break down when negative pressure results from them. Schemes possessing the important property of total variation diminishing, which was introduced by Harten [15], avoid non-physical oscillations near discontinuities. A TVD scheme can be second-order accurate except near extrema, where it degenerated to first order.

Many second-order TVD schemes have been proposed for scalar equations and Osher and Sweby [16] have classified them into pre-processing and post-processing types. A typical class of post-processing schemes are those obtained through flux limiters. In particular, Sweby [11] showed that the Van Leer scheme [17], the Chakravarthy and Osher scheme [18], the Roe scheme [19] are all derivable via suitable limiter functions.

To compute a flow solution to Eq. (1), a rectangular grid is used to cover the flow domain in the $\tau\xi$ plane and the computation marches in the Lagrangian time τ as in Part I. Any solid boundary present is represented by a streamline $\xi = \text{const}$. The superscripts n refers to the time step number

and subscript j refers to the cell number. The marching step, $\Delta\tau^n = \tau^{n+1} - \tau^n$, is uniform for all j excepts across a slip-line, where the marching step sizes $(\Delta\tau)_+$ and $(\Delta\tau)_-$ on the two sides of the slip-line are different, but are related by Eq. (7). The marching step may also vary with n but is always so chosen as to satisfy the usual CFL linear stability condition. The grid divides the computational domain into control volumes or cells (Fig. 1, Part I) which in the ξ-direction are centered at (τ^n, ξ_j) and have a width of $\Delta\xi_j = \xi_{j+1/2} - \xi_{j-1/2}$ for all n. Unless otherwise stated, we shall use uniform cell width, i.e., $\Delta\xi_j = h$ for all j.

The difference equations for the jth cell at time step n are formally derived by integrating Eq. (1) over that cell as in Part I to give

$$\mathbf{E}_j^{n+1} = \mathbf{E}_j^n - \frac{\Delta\tau^n}{\Delta\xi_j}[\mathbf{F}_{j+1/2}^{n+1/2} - \mathbf{F}_{j-1/2}^{n+1/2}]. \tag{8}$$

Here for any quantity g,

$$g_j^n = \frac{1}{\Delta\xi_j}\int_{\xi_{j-1/2}}^{\xi_{j+1/2}} g(\tau^n, \xi)\, d\xi \tag{9}$$

is the cell-average of g at time step n and

$$g_{j+1/2}^{n+1/2} = \frac{1}{\Delta\tau^n}\int_{\tau^n}^{\tau^{n+1}} g(\tau, \xi_{j+1/2})\, d\tau \tag{10}$$

is its time-average.

In the first-order Godunov scheme the flow in the jth cell at time step n is approximated by a uniform flow as given by its cell-average $\mathbf{E}_j^n$, and the flux $\mathbf{F}_{j+1/2}^{n+1/2}$ along the interface (a streamline) between the jth cell and the $(j+1)$th cell from time step n to $n+1$ is then obtained from the self-similar solution $\mathbf{R}((\xi - \xi_{j+1/2})/(\tau - \tau^n); \mathbf{Q}_j^n \mathbf{Q}_{j+1}^n)$ at $\xi = \xi_{j+1/2}$ to the Riemann problem formed by two adjacent uniform flow states $\mathbf{Q}_j^n$ and $\mathbf{Q}_{j+1}^n$. This flux will be denoted with a superscript G and the updating formula, Eq. (8), is written accordingly as

$$\mathbf{E}_j^{n+1} = \mathbf{E}_j^n - \lambda[(\mathbf{F}^G)_{j+1/2}^{n+1/2} - (\mathbf{F}^G)_{j-1/2}^{n+1/2}] \tag{11}$$

or

$$\mathbf{E}^{n+1} = \mathbf{E}_j^n - \lambda\Delta_-(\mathbf{F}^G)_{j+1/2}^{n+1/2}, \tag{12}$$

where

$$\Delta_- g_{j+1/2} = g_{j+1/2} - g_{j-1/2} \tag{13}$$

and $\lambda = \Delta\tau^n/\Delta\xi_j$. We note from Eq. (1) that the first two components of $\mathbf{E}$, e_1 and e_2, are constant for all τ and hence require no updating; the updating formula (11) applies only to e_3, e_4, e_5, and e_6.

To improve accuracy from the first-order Godunov scheme, we extend the second-order scalar TVD scheme of Sweby [11] in a component-by-component manner and propose the following updating formula for the system of Euler equations (1):

$$\begin{aligned}\mathbf{E}_j^{n+1} = \mathbf{E}_j^n &- \lambda\Delta_-(\mathbf{F}^G)_{j+1/2}^{n+1/2} \\ &- \lambda\Delta_-[\phi(r_j^+)\,\alpha_{j+1/2}^+(\Delta\mathbf{F}_{j+1/2})^+ \\ &- \phi(r_{j+1}^-)\,\alpha_{j+1/2}^-(\Delta\mathbf{F}_{j+1/2})^-]\end{aligned} \tag{14}$$

where

$$\begin{aligned}(\Delta\mathbf{F}_{j+1/2})^+ &= \mathbf{F}(\mathbf{Q}_{j+1}^n) - (\mathbf{F}^G)_{j+1/2}^{n+1/2} \\ (\Delta\mathbf{F}_{j+1/2})^- &= (\mathbf{F}^G)_{j+1/2}^{n+1/2} - \mathbf{F}(\mathbf{Q}_j^n) \\ \alpha_{j+1/2}^{\pm} &= \tfrac{1}{2}(1 \mp v_{j+1/2}^{\pm}) \\ v_{j+1/2}^{\pm} &= \lambda(\Delta(f_i)_{j+1/2})^{\pm}/[(e_i)_{j+1}^n - (e_i)_j^n] \\ &\qquad (i = 3, 4, 5, 6)\end{aligned} \tag{15}$$

and

$$r_j^{\pm} = \left[\frac{\alpha_{j-1/2}^{\pm}(\Delta(f_i)_{j-1/2})^{\pm}}{\alpha_{j+1/2}^{\pm}(\Delta(f_i)_{j+1/2})^{\pm}}\right]^{\pm 1} \quad (i = 3, 4, 5, 6). \tag{16}$$

Equation (14) was derived [11] for the special case when $\mathbf{E}$ is a scalar. We have applied it to the Euler equations (1) for each component e_3, e_4, e_5, and e_6 separately. For instance, to update the third component e_3 from time step n to $n+1$ all quantities on the RHS of (14) are evaluated using $(e_3)_j^n$ for $\mathbf{E}_j^n$ and $(f_3)_j^n$ for $\mathbf{F}_j^n$. Once $\mathbf{E}_j^{n+1}$ is calculated via (14) the same decoding procedure as in Part I is then used to compute the flow state $\mathbf{Q}_j^{n+1}$ and the updating process is repeated to the next time step $n+2$, and so on and so forth.

In Eq. (14), $\phi = \phi(r)$ is the limiter function. $\phi = 0$ reduces (14) to the first-order Godunov scheme, whereas $\phi = 1$ yields the conventional second-order Lax–Wendroff scheme which produces non-physical oscillations around discontinuities. The idea of flux limiter is to suitably choose $\phi(r)$ so that (14) is total variation diminishing while hoping to retain second-order accuracy in most parts of the continuous flow regions except at extrema, where it degenerates to first order. It is this TVD property that removes the non-physical oscillations. Several flux limiter schemes have been proposed and, as mentioned earlier, Sweby [11] has shown that they amount to different choices of the limiter function $\phi(r)$. Our numerical experiments using the limiters of Van Leer [17], Chakravarthy and Osher [18], Roe [19], and Sweby [11] show that there is little difference between

them. All results presented in this paper have been obtained using Van Leer limiter for which

$$\phi(r)=\begin{cases}0 & (r\leqslant 0)\\ \dfrac{2r}{1+r} & (r>0)\end{cases} \tag{17}$$

For the scalar case, second-order accuracy of scheme (14) is attained [11]. The simple extension of the scheme to the system of Euler equations as explained above does not theoretically assure its second-order accuracy. But our numerical experiments have shown (see Figs. 8 and 11 below) that it is much more accurate than the first-order Godunov scheme, and we shall call it a high resolution TVD scheme.

As seen from the structure of (14)–(16), to update $\mathbf{E}_j$ from time step n to $n+1$ with high resolution requires knowledge of five computational cells: $\mathbf{E}^n_{j-2}$, $\mathbf{E}^n_{j-1}$, $\mathbf{E}^n_j$, $\mathbf{E}^n_{j+1}$, and $\mathbf{E}^n_{j+2}$, whereas the first-order Godunov scheme requires only three: $\mathbf{E}^n_{j-1}$, $\mathbf{E}^n_j$, and $\mathbf{E}^n_{j+1}$. Whilst the requirement of a stencil of five computational cells, instead of three, causes no difficulty for purely initial value problems, it does present some problems when a solid boundary is present in the flow. The special treatment required at the solid boundary will be discussed now.

3.2. *Sub-cell Treatment for Smooth Walls*

Let the cell adjacent to the wall be denoted by $j=1$. At time step n, $\mathbf{E}^n_j$ is known for $j=1, 2, 3, \ldots$, so the updating formula (14) can be readily used to obtain $\mathbf{E}^{n+1}_j$ for $j=3, 4, 5, \ldots$, but not so for $j=1$ and 2. At the wall the flow direction θ is given, and the flow tangency condition there can be satisfied by introducing a fictious cell, $j=0$; on the other side of the wall which is the mirror image of the flow of the cell, $j=1$ with respect to the wall tangent plane. (The application of this reflection principle was noted in Part I to be equivalent to solving a boundary Riemann problem.) The introduction of this fictitous cell $j=0$ allows us to apply the high resolution updating formula (14) also for $j=2$, leaving the updating of the boundary cell, $j=1$, at first-order accuracy.

To have the same accuracy for the boundary cell requires a knowledge of an additional cell, $j=-1$, below the cell $j=0$ which, it might be thought, could easily be obtained by extrapolation. Unfortunately, our computer experiments with various seemingly reasonable extrapolations prove fruitless; rather they tend to confirm the observation of Vinokur [20] that at solid boundaries a first-order scheme is preferable to a second-order one in preventing unphysical results.

However, in a given supersonic stream past a solid body it is the body shape that determines the subsequent development of the flow. It is, therefore, important to be able to compute the flow near the solid boundary more accurately than the first order. This can be done by following the boundary shape more closely. We have found that a sub-cell treatment for the boundary cell serves this purpose very well. The procedure is as follows. To obtain an improved $\mathbf{E}^{n+1}_1$ the width h of the original cell AB (Fig. 4) at time step n is divided into m equal sub-cells of width h/m. The first-order Godunov scheme is then applied to compute the time evolution of these subcell flows by marching with sub-time $\Delta\tau/m$, $\Delta\tau$ being the original time step. In doing so the interface flux originally calculated along the cell upper boundary AD is used as the flux along AA_1, while for the flux along the body surface the surface slope of BB_1 is used (in the boundary Riemann solver) instead of the original slope of BC. This process is repeated m times until the original time step $n+1$ is reached, during which the upper interface flux is held to be the same as that given by the original flux along AD, but the surface slope assumes its *local* values at the sub-segments BB_1, B_1B_2, ..., $B_{n-1}B_n$. After the last sub-time step, $\mathbf{E}^{n+1}_{1i}$ $(i=1, 2, \ldots, m)$ are obtained and the arithmetic average is then taken to yield

$$\mathbf{E}^{n+1}_1=\frac{1}{m}\sum_{i=1}^{m}\mathbf{E}^{n+1}_{1i} \tag{18}$$

This completes the sub-cell treatment for the boundary cell from time step n to $n+1$. The computation can then be marched as usual from time step $n+1$ to $n+2$, again with sub-cell treatment for the boundary cell.

It is clear from the description above that the sub-cell treatment inputs more details of the curved boundary shape to the flow field, but is ineffective and hence not useful for flat boundaries. In this paper it is employed in Figs. 5 and 10 only. The sub-cell treatment for the boundary cell is very easy to implement and, with $m=O(1/h^{1/2})$, the accuracy of the computed flow in the boundary cell is found to be typically improved to the same level as the interior cells. An example is given in Fig. 5 in which the supersonic flow of $M_\infty=3$ is expanding over the wall shape $y=-x^2$. Fifty uniform cells with $h=0.002$, $m=10$ are used in the computation. It is seen from these figures that the pressure can

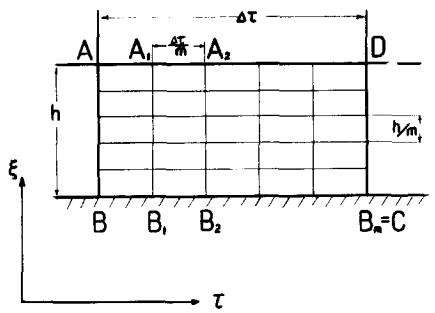

FIG. 4. Boundary sub-cells.

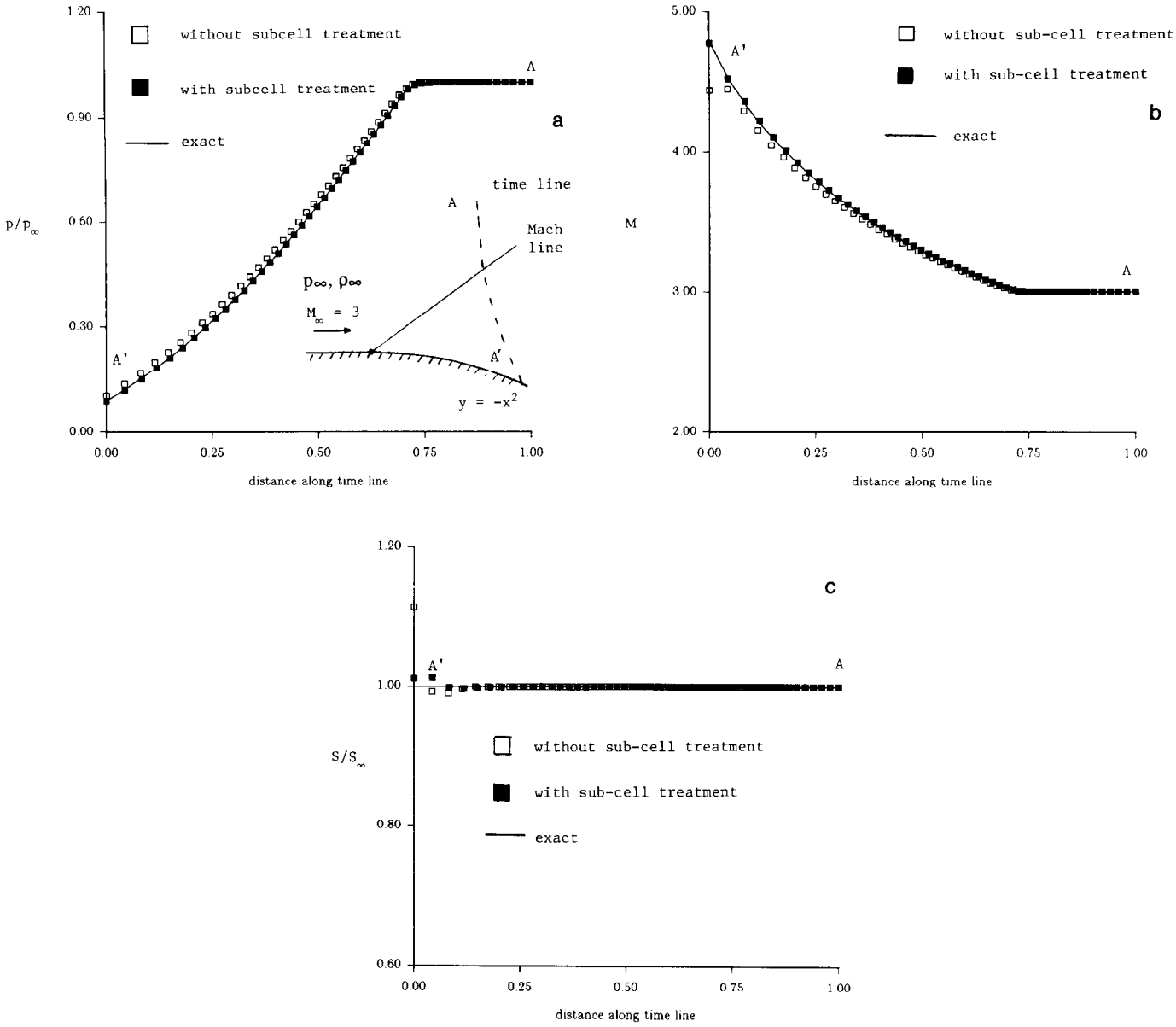

FIG. 5. Flow variables along a typical time line AA', in an expansion flow over a smooth surface. Computed from (14)–(17) with $h = 0.002$, $m = 10$: (a) pressure; (b) Mach number; (c) entropy.

be computed accurately without a sub-cell treatment, but for Mach number and entropy a sub-cell treatment is necessary to bring the accuracy of the high resolution TVD scheme more uniformly. This result is also typical of general flow field computation in that pressure is a flow variable which can be computed very accurately, but entropy should be the one to use for critically testing the accuracy of a numerical method.

3.3. *Special Procedure for Wall-Corner*

The presence of a corner at the wall generates singular behavior of the flow field near the corner. In Part I, special procedures were devised for numerically treating the singularity. With the high resolution TVD scheme equations (14)–(17) we have found that the procedure for treating an expansion corner can be simplified, yielding somewhat more accurate results, as follows:

(a) Adjust time step size so that the turning corner is hit exactly by a grid time line.

(b) Use the flow state $\mathbf{Q}_u$, U_u, V_u immediately upstream of the corner to calculate that immediately downstream of it, the latter being denoted as $\mathbf{Q}_d$, U_d, V_d. This is done by using the Prandtl–Meyer exact solution in Lagrangian form

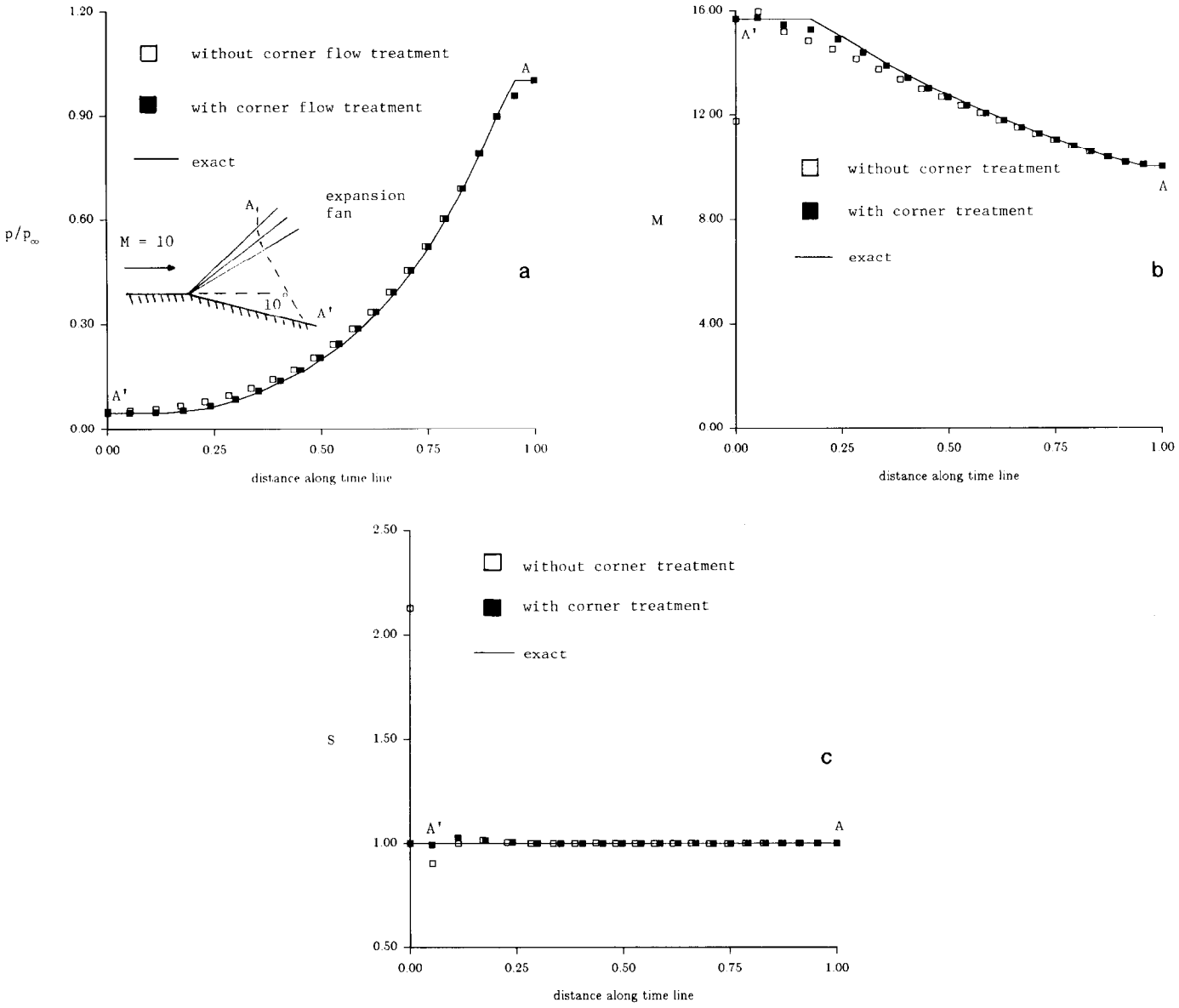

FIG. 6. Prandtl–Meyer flow, $M = 10$, $\alpha = 10°$, computed flow variables along a typical time-line AA', from (14)–(17). No sub-cell treatment. (a) pressure; (b) Mach number; (c) entropy.

(Part I); in particular, U_d and V_d are obtained by integration along a streamline.

(c) Applying the updating formula (14) as usual until the wall cell falls completely downstream of the Prandtl–Meyer expansion fan. Then replace the numerically calculated $\mathbf{Q}$, U, V for the wall cell by $\mathbf{Q}_d$, U_d, V_d and terminate the special procedure.

Systematic computations of supersonic flow M past an expansion corner angle α, for various combinations of M and α, show that this special procedure usually leads to error in entropy of less than about 2% when compared with the exact Prandtl–Meyer solution. Figures 6 plot the results of the case of $M = 10$ and $\alpha = 10°$ which clearly show that the special treatment for a corner is essential for getting accurate results for wall density, Mach number, and entropy. No sub-cell treatment was applied here. The present results are also seen to be slightly more accurate than those of Glaz and Wardlaw based on Eulerian formulation. For instance, with the same number of 22 cells their computed Mach number has a maximum error of 6% (Fig. 10 of [3]), compared to 2.5% in ours (Fig. 6b).

4. EXAMPLES

Four examples are given in this section to show the capability of the high resolution TVD scheme equations

(14)–(17) based on the new Lagrangian formulation in resolving shock and slip-line discontinuity and in improving the accuracy of continuous flow. This will be demonstrated by comparison with exact solutions, with the first-order Godunov scheme, and with the second-order scheme of Glaz and Wardlaw based on the Eulerian formulation. In all these examples, except Fig. 10, no sub-cell treatment was employed.

The first example is the interaction of two shocks which was first computed by Glaz and Wardlaw [3]. The shock–shock interaction is generated by a flow of $M = 10$ in a converging channel containing both upper and lower wall slope discontinuities at 10° and 20°, respectively. The collision of the two shocks belonging to different families produces two new shocks and a slip-line. Figures 7a–b show the pressure and density distributions along a typical time-line after the collision as computed from Eqs. (14)–(17) with no special procedure for slip-line detection. The exact solution (solid line) is also plotted for comparison, and the agreement is seen to be very good. By comparison with the first-order results of Part I, it is seen that the resolutions of shocks and slip-line are significantly improved. The high resolution TVD scheme equations (14)–(17), with no sub-cell treatment, take a maximum of two cells to cross a shock and only one to cross the slip-line, compared with six and two, respectively, for the first-order Godunov scheme. Furthermore, comparisons with the second-order scheme of Glaz and Wardlaw [3, Fig. 17] in Eulerian formulation show that both methods attain the same level of shock resolution whilst the slip-line is much better resolved in the new Lagrangian formulation.

The second example is the Riemann problem No. 1 computed in Fig. 6 of Part I recomputed using the present TVD scheme equations (14)–(17). The results for pressure and

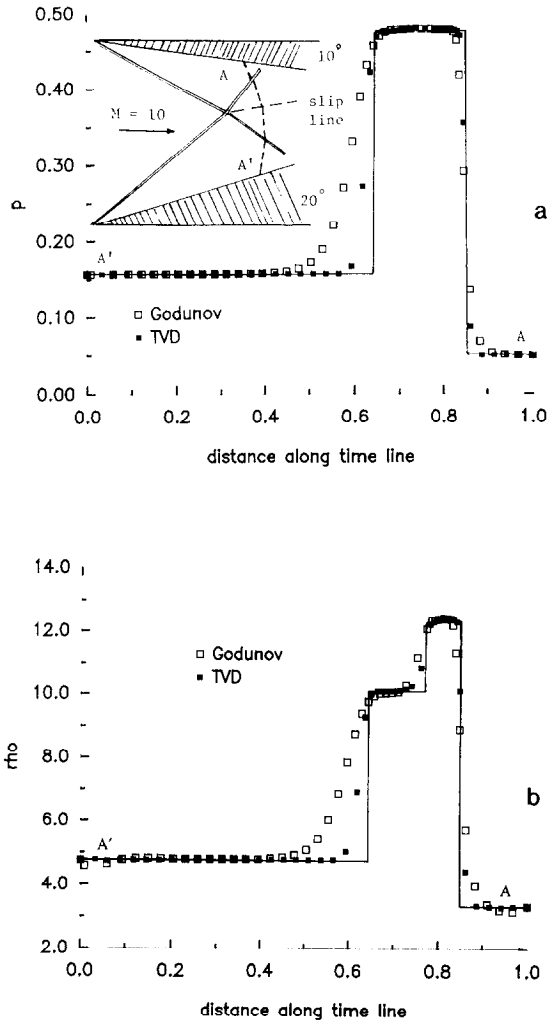

FIG. 7. Shock–shock interaction problem. Computed variables along a typical time-line AA', from (14)–(17). No sub-cell treatment. (a) pressure; (b) density. Solid line denotes exact solution.

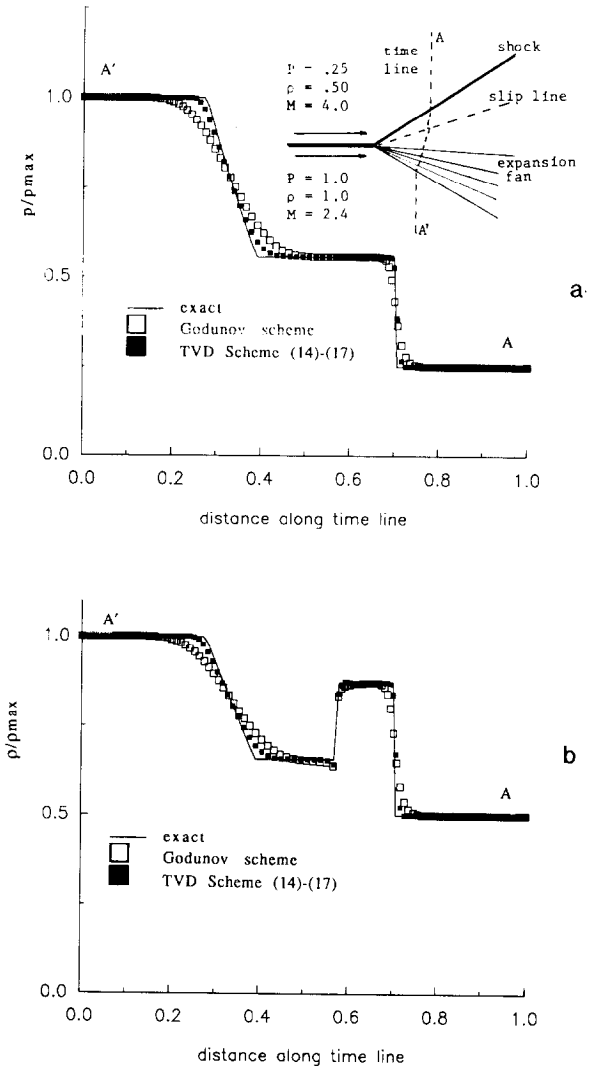

FIG. 8. Pressure and density distributions along a time-line AA' in a Riemann problem computed using (14)–(17): (a) pressure; (b) density. No sub-cell treatment.

density distributions along a typical time line are plotted in Fig. 8. It is clear from comparisons with exact solutions in these figures that the high resolution TVD scheme is a significant improvement over the first-order Godunov scheme in the continuous flow region, while it also improves somewhat in shock resolution.

In the third example we compute a supersonic flow $M_0 > 1$ past a concave wall for which a shock of finite strength is formed suddenly in the interior of the flow field and consequently a slip-line is also generated. The shape of the wall is given (see Appendix A) parametrically as

$$\Gamma: \begin{cases} \dfrac{x(M)}{l} = 1 - \dfrac{G(M)\cos\{\phi(M) - \phi(M_0) + \mu_0\}}{G(M_0)\cos\mu_0} \\ \qquad (M_1 < M \leqslant M_0), \\ \dfrac{y(M)}{l} = \tan\mu_0\left[1 - \dfrac{G(M)\sin\{\phi(M) - \phi(M_0) + \mu_0\}}{G(M_0)\sin\mu_0}\right] \\ \qquad (M_1 < M \leqslant M_0) \end{cases} \tag{18a}$$

on the curve part, followed by a straight line tangent to it at the point corresponding to $M = M_1 > 1$, the equation of which is

$$\frac{y - y(M_1)}{x - x(M_1)} = \tan[\phi(M_1) - \phi(M_0) - \mu_1 + \mu_0]$$
$$(1 \leqslant M \leqslant M_1), \tag{18b}$$

where l is an arbitrary length scale which is taken to be equal to 1, M is flow Mach number, and

$$\mu = \sin^{-1}\frac{1}{M}$$

$$G(M) = \left[1 + \frac{\gamma - 1}{2}M^2\right]^{((\gamma+1)/(\gamma-1))/2}$$

$$\phi(M) = \sqrt{(\gamma+1)/(\gamma-1)} \times \tan^{-1}[\sqrt{(\gamma+1)/(\gamma-1)}/\sqrt{M^2 - 1}].$$

The family of curves Γ for different M_0 but with $M_1 = 1$ are plotted in Fig. 9. From any of these curves one can construct a wall shape consisting of a concave forward portion Γ for $1 < M_1 < M \leqslant M_0$ followed by a straight line tangent to Γ at its end point $(x(M_1), y(M_1))$. When this shape is placed in a supersonic uniform stream M_0 with its leading edge aligned to the stream, the flow is compressed in a particular manner such that a shock of finite strength is produced suddenly at $P_0(1, \tan\mu_0)$. At the same moment, a slip-line is also generated at the same point (see Fig. 10a). The exact solution to this flow is obtainable via Riemann invariants for the continuous part and via the Riemann problem at shock birth.

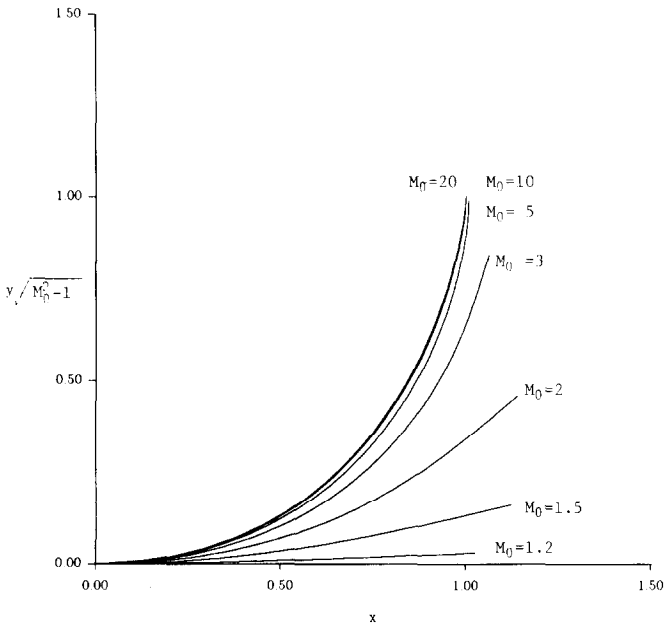

FIG. 9. Concave curves Γ that generate a shock of finite strength suddenly Eq. (18a) $(1 < M < M_0)$.

To illustrate, we consider the case when $M_0 = 4$ and $M_1 = 2.867$. The flow field is computed using the high resolution TVD scheme equations (14)–(17) with 50 cells $(h = 0.015)$ plus sub-cell treatment $(m = 10)$ on the wall cell. In Figs. 10b–d the computed isobars, density contours, and entropy contours are plotted. The sudden birth of a shock of finite strength in the interior of the flow field and the accompanying slip-line are seen well-captured. These figures also show the weak expansion can centered at the point of shock birth and its reflection by the plane wall. Figures 10e–f show the computed distributions of pressure and Mach number along a typical time line AA' downstream of the shock birth but before the expansion waves reach the plane wall. They are seen to be in very good agreement with the exact solution (solid line in the figures), in particular, both shock and slip-line are resolved in two grid points.

In the last example[1] we compute the flow due to a strong shock impinging on a slip-line. The shock is generated by a hypersonic flow of Mach 10 passing over a wedge of 20°. After the shock impinges on a slip-line, both the shock and the slip-line are deflected while a Prandtl–Meyer expansion

[1] We are grateful for the reviewer who suggests this example as a test case.

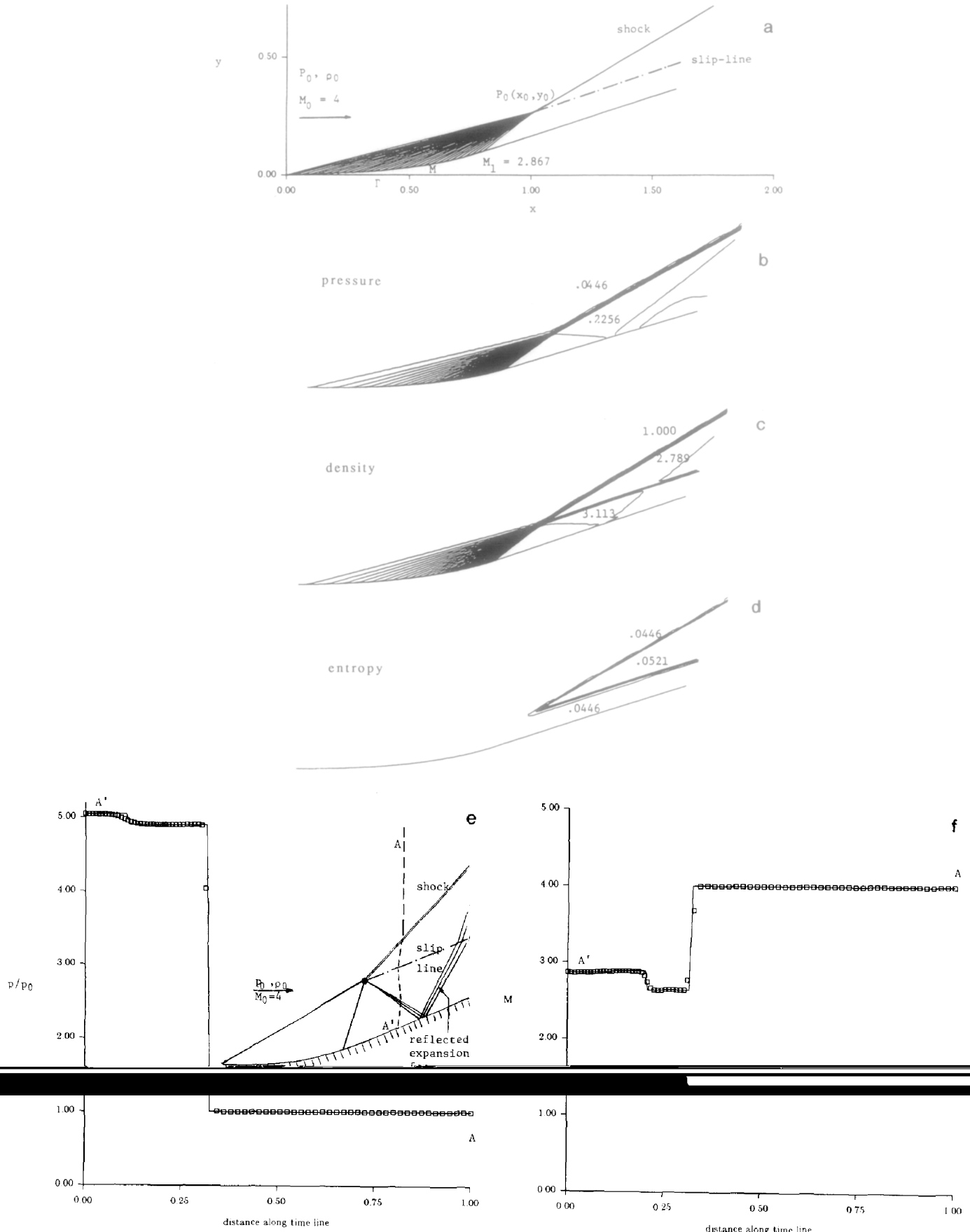

FIG. 10. (a) Computed pre-shock Mach lines for a $M_0 = 4$ flow past the Γ curve body with $M_1 = 2.867$, with sub-cell treatment, $m = 10$, $h = 0.015$; (b) computed isobars; (c) computed density contours; and (d) computed entropy contours; (e)–(f) computed flow variables along a typical time line AA': (e) pressure; (f) Mach number. Solid line denotes exact solution.

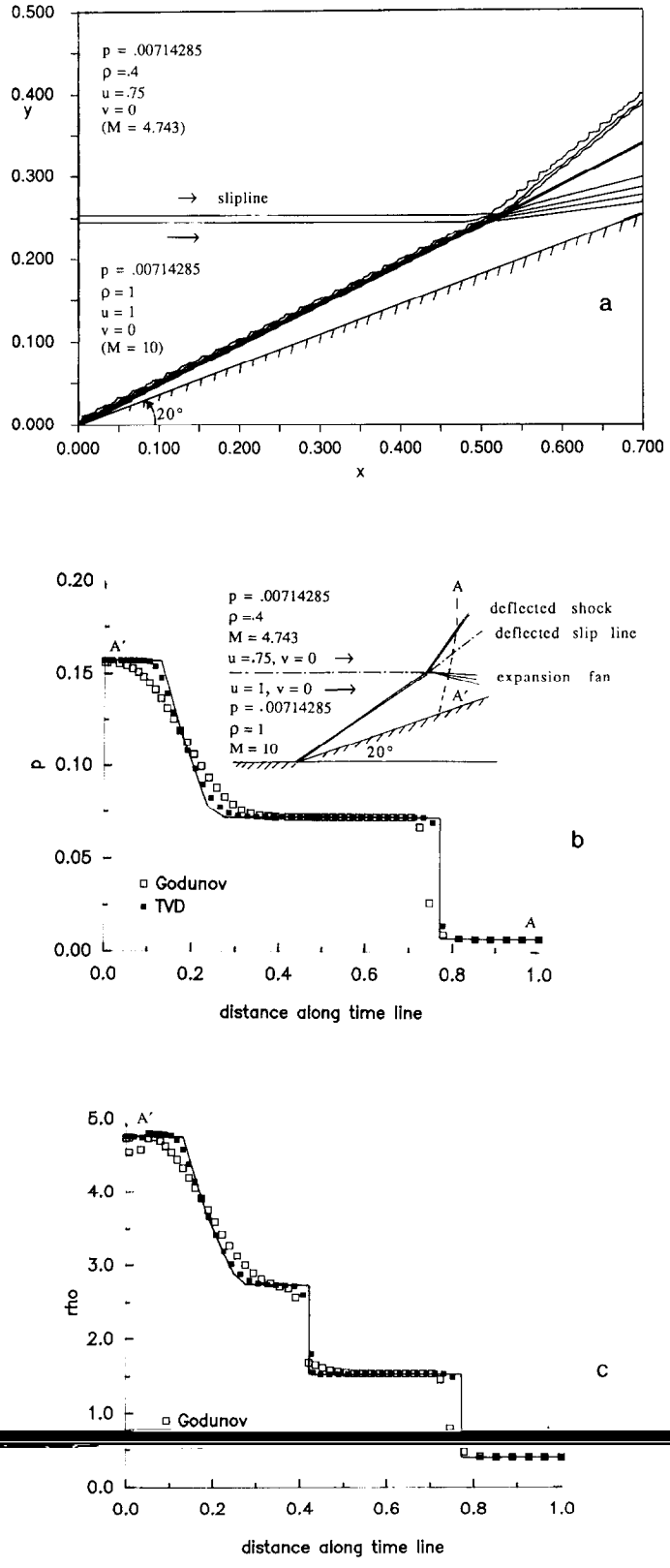

FIG. 11. Computed, using (14)–(17), flow due to a shock impinging on a slip-line, 50 cells, $h = 0.01$: (a) density contours; (b) pressure distribution along a time line AA'; (c) density distribution along a time line AA'. No sub-cell treatment.

fan is generated. With 50 cells of width $h = 0.01$, the computed density contours are shown in Fig. 11a, whereas the computed pressure and density distributions along a time line AA' after the impingement are shown in Figs. 11b, c. Agreements with exact solutions are, again, seen to be very good; in particular, both shock and slip-line discontinuities are seen resolved to within two grid points.

5. CONCLUSIONS

It has been shown in this paper that the new Lagrangian formulation of Hui and Van Roessel plus Godunov scheme is capable of resolving an isolated slip-line discontinuity in steady supersonic flow crisply, provided it is initially aligned with a computational grid line. It has further been shown that the high resolution TVD scheme equations (14)–(17) based on the new Lagrangian formulation, with no special procedure for slip-line detection, are very accurate and resolve both shock and slip-line discontinuities to within two grid points. This is achieved despite the slip line being a linearly degenerated field. Moreover, in the new Lagrangian formulation using stream-lines as coordinate lines there is no need for grid generation to fit a given body shape, as is required in Eulerian formulation. In these regards, the new Lagrangian method is evidently superior to the Eulerian method for computing steady supersonic flow of an inviscid gas. We also note that the Lagrangian method was used recently by So and Zhang [21] with success to help resolve slip-line discontinuity in their overall Eulerian formulation. They re-map to Eulerian description at each time step. By contrast, the present method is entirely Lagrangian and no re-map is necessary.

APPENDIX A: EXACT SUPERSONIC FLOW WITH SUDDEN FORMATION OF SHOCK WAVE

W. H. Hui and Y. C. Zhao

It is well known that when a supersonic flow encounters a concave solid wall it is compressed by the wall and a shock wave will be formed. If the wall has a corner—surface slope discontinuity—a shock wave of finite strength is formed at the corner and extended into the flow field. If, on the other hand, the wall is smooth a shock wave is formed in the interior of the flow field and, in general, it is formed gradually along the envelop of the converging Mach lines with infinitesimal strength at its birth point.

Here we set out to determine families of smooth wall shape Γ whose compression effects on the supersonic flow lead to sudden formation of a shock of finite strength in the interior of the flow field.

Let the steady uniform supersonic stream $M_0 > 1$ be aligned with the x-direction in the cartesian xy plane

(Fig. 9a). Let the sought-for wall shape Γ be given parametrically as

$$x = x(\theta), \qquad z = y(\theta), \tag{A1}$$

where θ is the inclination of its tangent, whence

$$\frac{dy}{d\theta} = \frac{dx}{d\theta}\tan\theta. \tag{A2}$$

We also choose the origin of the coordinate system so that

$$x(0) = y(0) = 0. \tag{A3}$$

Let $P_0(x_0, y_0)$ be the point where the shock of finite strength is first formed. Then, clearly, every straight line joining P_0 to a point $M(x(\theta), y(\theta))$ on Γ is a Mach line of the flow. Hence

$$y(\theta) - y_0 = [x(\theta) - x_0]\tan(\theta + \mu), \tag{A4}$$

where

$$\mu = \sin^{-1}\frac{1}{M} \tag{A5}$$

is the Mach angle and M is the flow Mach number. At $\theta = 0$, Eq. (A4) yields

$$y_0 = x_0 \tan\mu_0 \tag{A6}$$

Elimination of $y(\theta)$ from (A2) and (A4) gives

$$\frac{dx}{d\theta}[\tan(\theta+\mu) - \tan\theta] = [x_0 - x(\theta)]\frac{d}{d\theta}\tan(\theta+\mu) \tag{A7}$$

whose solution is

$$x = x_0(1 - e^{-I(\theta)}), \tag{A8}$$

where

$$I(\theta) = \int_0^\theta \frac{1}{\tan(\theta+\mu) - \tan\theta}\frac{d}{d\theta}\tan(\theta+\mu)\,d\theta. \tag{A9}$$

Since prior to shock formation the flow is a simple wave, we have (see Whitham [21])

$$\theta = P(\mu) - P(\mu_0), \tag{A10}$$

where

$$P(\mu) = \sqrt{(\gamma+1)/(\gamma-1)}\tan^{-1}(\sqrt{(\gamma+1)/(\gamma-1)}\tan\mu) - \mu \tag{A11}$$

and γ is the ratio of specific heats of the gas.

By use of (A10) and (A11), the RHS of (A9) can be integrated out explicitly. The results for x and y, when expressed as functions of M, are given in Eq. (18a), where the arbitrary constant x_0 has been replaced by l.

For a given $M_0 > 0$, there is a unique curve Γ defined in Eq. (18a) for $1 < M \leqslant M_0$. A wall shape can be constructed for any given M_0 with $M_1 > 1$ and $M_1 < M_0$, by using the forward portion of Γ for $M_1 < M \leqslant M_0$ followed by a straight line tangent to Γ at its end point M_1 whose equation is given by Eq. (18b). Such a shape for $M_0 = 4$ and $M_1 = 2.867$ is shown in Fig. 9a.

Exact solution to steady supersonic flow $M_0 > 1$ past any wall shape constructed above with $M_1 > 1$ can be obtained easily. In the fan region centered at $P_0(x_0, y_0)$ the flow is a simple wave and is given by Eqs. (A10) and (A11), together with the fact that along each Mach line P_0M all the flow variables are constant. At the point of shock formation P_0 we have a Riemann problem: the uniform flow M_0 above P and a uniform flow (that on P_0M_1) below it. The solution to the Riemann problem is well known.

If the simpler case of one-dimensional unsteady flow we may also determine the motion of a piston $x = x(t)$ toward a gas at rest with t being the time variable, such that a shock wave of finite strength will be formed, due to compression of the piston, in the interior of the flow field. Applying similar arguments as above, we obtain

$$x(t) = \frac{\gamma+1}{\gamma-1}a_0 t_0\left[1 - \frac{2}{\gamma+1}\frac{t}{t_0} - \left(1 - \frac{t}{t_0}\right)^{2/(\gamma+1)}\right] \qquad (0 \leqslant t < t_0), \tag{A12}$$

where a_0 is the speed of sound of the undisturbed gas. The shock of finite strength is formed suddenly at time t_0 beginnin at $x_0 = a_0 t_0$. A slip-line (contact-line) is also produced simultaneously at $x = x_0$ and $t = t_0$. The unsteady flow field of the gas resulting from the motion of the piston can also be calculated exactly using Riemann invariants for the continuous part for $t < t_0$ and by solving the Riemann problem at $t = t_0$ when the shock is suddenly formed.

The strength of the shock and contact line can be varied by varying a_0 and t_0. It would be interesting to see how accurate the many existing shock-capturing schemes for one-dimensional unsteady flow are in reproducing this exact solution to an initial-boundary value problem, in addition to Sod's famous shock-tube initial value problem where the position of the contact line is known initially.

ACKNOWLEDGMENTS

This research was supported by a grant from the Natural Science and Engineering Research Council of Canada awarded to W. H. Hui and an NSERC Postdoctoral Fellowship to C. Y. Loh. The computations for this paper were carried out using the Cray X-MP computer at the Ontario Center for Large Scale Computation.

REFERENCES

1. H. C. Yee, A class of high resolution explicit and implicit shock capturing methods, in *VKI for Fluid Dynamics Lecture Series* 1989-04, Vol. 1 (1989).
2. P. L. Roe, The influence of mesh quality on solution accuracy, in *VKI for Fluid Dynamics Lecture Series* 1989-04, Vol. 1 (1989).
3. H. M. Glaz and A. B. Wardlaw, *J. Comput. Phys.* **58**, 157 (1985).
4. M. Pandolfi, *Comput. & Fluids* **10**, 37 (1985).
5. P. Woodward and P. Colella, *J. Comput. Phys.* **54**, 14 (1984).
6. A. Harten, in *Wave Motion: Theory, Modelling, and Computation*, edited by A. J. Chorin and A. J. Majda (Springer-Verlag, New York/Berlin, 1987), p. 147.
7. M. S. Liou, B. Van Leer, and J. S. Shuen, *J. Comput. Phys.* **87**, 1 (1990).
8. W. H. Hui and H. J. Van Roessel, in *NATO AGARD Symposium on Unsteady Aerodynamics—Fundamentals and Application to Aircraft Dynamics, Gottingen, Germany, 6–9 May, 1985*, CP-386 (AGARD, 1985), paper #S1.
9. H. J. Van Roessel and W. H. Hui, A new Lagrangian formulation for steady three-dimensional hypersonic flow, *J. Appl. Math. Phys.* **40**, 677 (1989).
10. C. Y. Loh and W. H. Hui, *J. Comput. Phys.* **89**, 207 (1990).
11. P. K. Sweby, *SIAM Numer. Anal.* **21**, 995 (1984).
12. A. Harten, *Pure Appl. Math.* **30**, 611 (1977).
13. C. W. Shu and S. Osher, *J. Comput. Phys.* **83**, 32 (1989).
14. A. Harten, *J. Comput. Phys.* **83**, 148 (1989).
15. A. Harten, *Math. Comput.* **32**, 363 (1978).
16. S. Osher and P. K. Sweby, Recent developments in the numerical solution of non-linear conservation laws, 1986 (unpublished).
17. B. Van Leer, *J. Comput. Phys.* **14**, 361 (1974).
18. S. Chakravarthy and S. Osher, in *Proceedings, 8th CDF Conference, 1983*; AIAA Paper, 831943.
19. P. L. Roe, Some contribution to the modelling of discontinuous flow, in *Lecture, QMS–SIAM Summer Seminar on Large Scale Computation in Fluid Dynamics, Univ. of Calif., San Diego, July 1983* (Amer. Math. Soc., Providence, RI, 1985).
20. M. Vinokur, *J. Comput. Phys.* **81**, 1 (1989).
21. R. M. C. So and H. S. Zhang, A flux coordinates splitting technique for Navier–Stokes equations, *AIAA J.*, June (1991).
22. G. B. Whitham, *Linear and Nonlinear Waves* (Wiley, New York, 1974), p. 203.